

## Observation of Stable Superdense Core Plasmas in the Large Helical Device

N. Ohyaibu, T. Morisaki, S. Masuzaki, R. Sakamoto, M. Kobayashi, J. Miyazawa, M. Shoji, A. Komori, O. Motojima, and LHD Experimental Group  
National Institute for Fusion Science, Toki 509-5292, Japan  
(Received 25 May 2006; published 3 August 2006)

In reduced recycling discharges in the Large Helical Device, a super dense core plasma develops when a series of pellets are injected. A core region with density as high as  $4.5 \times 10^{20} \text{ m}^{-3}$  and temperature of 0.85 keV is maintained by an internal diffusion barrier with very high-density gradient. These results may extrapolate to a scenario for fusion ignition at very high density and relatively low temperature in helical devices.

DOI: [10.1103/PhysRevLett.97.055002](https://doi.org/10.1103/PhysRevLett.97.055002)

PACS numbers: 52.55.Hc

Improvement of plasma particle and energy confinement is a major challenge for toroidal magnetic fusion research, and will be important in igniting burning plasmas in ITER [1]. Various confinement improvement modes have been discovered including edge transport barriers (ETBs, or *H* mode) [2] and internal transport barriers (ITBs) [3–5]. In this Letter, we describe improved confinement in super dense core (SDC) plasmas, in diverted discharges in the Large Helical Device (LHD), a heliotron configuration in which the rotational transform is provided by external magnetic coils. This operational regime may extrapolate to a high-density, relatively low temperature ignition scenario for these devices.

LHD has an external helical field with poloidal winding number  $l = 2$  and  $M = 10$  toroidal field periods. The major radius of the magnetic axis,  $R_{\text{ax}} = 3.5\text{--}3.9$  m, average plasma minor radius  $a \sim 0.6$  m, and toroidal magnetic field  $B \leq 3.0$  T [6]. Depending on the relative currents in the helical and auxiliary poloidal coils, the rotational transform on axis,  $\iota(0)/2\pi = 0.3\text{--}0.6$  and the edge transform,  $\iota(a)/2\pi = 1\text{--}1.5$ .

One of the major goals of the LHD program is the demonstration of a reactor-relevant, diverted helical plasma. Two different divertor systems are available in LHD: the Helical Divertor (HD) [7] and the Local Island Divertor (LID) [8–10]. The HD is an intrinsic helical double-null divertor with an open divertor geometry, essentially like a helically twisting double-null tokamak poloidal divertor. The LID uses an  $m = 1$ ,  $n = 1$  resonant magnetic island (poloidal and toroidal mode numbers  $m$  and  $n$ , respectively) to guide particle and heat fluxes to divertor plates.

A SDC plasma develops spontaneously in LHD as a highly peaked density profile is created by injection of multiple pellets from the outside midplane as illustrated in Fig. 1(a). The density and temperature profiles are depicted for the standard ( $R_{\text{ax}} = 3.75$  m,  $B = 2.64$  T,  $P = 10$  MW) discharge diverted by the LID in Fig. 1(b). These profiles are measured using a Thomson scattering diagnos-

tic along  $R_{\text{horiz}}$ , the major radius in the poloidal plane where the plasma is horizontally elongated [Fig. 1(a)]. A core region with electron density  $\leq 4.5 \times 10^{20} \text{ m}^{-3}$  and temperatures  $\sim 0.85$  keV is maintained by an internal diffusion barrier (IDB) located at normalized minor radius  $\rho \sim 0.5$ . The radial width of the IDB is  $\sim 0.10$  m ( $\Delta\rho \sim 0.2$ ). The density gradient at the IDB is extremely high ( $\nabla n \sim 2.5 \times 10^{21} \text{ m}^{-4}$ ). Inside the SDC region, the density and temperature gradients are nearly zero. The density gradient outside the IDB is weak, with  $n(\rho = 1) \sim 5 \times 10^{19} \text{ m}^{-3}$ .

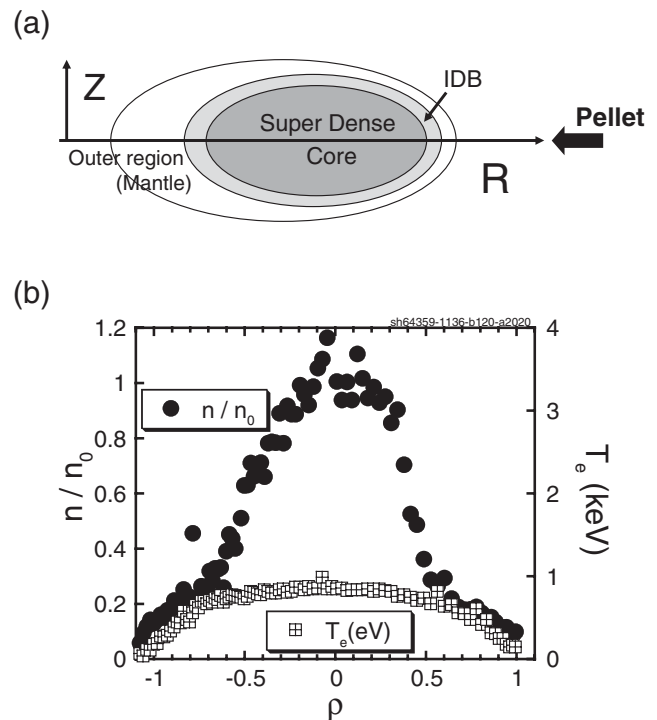


FIG. 1. (a) Illustration of a SDC plasma. (b) Density and temperature profiles of an SDC discharge with  $R_{\text{ax}} = 3.75$  m are depicted. The density normalization factor  $n_0 = 4.5 \times 10^{20} \text{ m}^{-3}$ ,  $P = 10$  MW.

SDC discharges exhibit the highest fusion plasma performance achieved so far on LHD,  $n_0 T_0 \tau_E \sim 4.4 \times 10^{19}$  keV m<sup>-3</sup> s, despite a  $\sim 40\%$  reduction in effective confinement volume (due to the LID) from standard HD discharges. In SDC experiments so far,  $\beta(0)$ , beta value at the center = 4.4% (5.1%) at  $B = 2.64$  T (1.5 T). Even with the relatively high  $\beta$ , neither macroscopic MHD instabilities nor beta collapse are seen. This is quite different from improved confinement modes in tokamaks in which MHD phenomena limit the achievable  $\beta$  [11,12].

The production of the SDC begins with sequential injection of 6 or more pellets which penetrate beyond the magnetic axis and drive the formation of a strongly peaked density profile. We use 10 pellet barrels [4 barrels with  $\Delta N$ (total number of particle/barrel) =  $1 \times 10^{21}$ , 3 with  $\Delta N = 2 \times 10^{21}$ , 3 with  $\Delta N = 3 \times 10^{21}$ ] and continuous pellet injector ( $\Delta N = 1 \times 10^{21}$ , interval  $\geq 100$  msec) [13]. Figure 2 shows how the injection of a series of pellets, each producing a spike on the  $H_\alpha$  diagnostic, raises the density. The initial density profile is flat. At  $t = 780$  ms, the profile takes on a peaked shape. Subsequent pellets raise the density while retaining the peaked shape characteristic of SDC plasmas (Fig. 1). After  $t = 940$  ms, when the last pellet is injected,  $n(0)$  decays continuously with a time constant  $\sim 1$  s, indicating that the diffusion coefficient in the IDB is less than  $0.02$  m<sup>2</sup> s<sup>-1</sup>.  $W_p$  decreases slightly and at  $t = 955$  ms,  $W_p$  starts to increase—the relative increase in temperature is greater than the simultaneous decrease in density—and reaches its maximum value at  $t = 1100$  ms. Similar behavior has been observed in so-called “reheat events” [14]. SDC plasmas, however, can be maintained by continued pellet injection.

SDC plasmas cannot be obtained in discharges fueled by gas puffing alone, because edge recycling results in a broad, flat, or slightly hollow density profile. The use of the LID increases pumping of edge-recycled particles and maintains low edge density and high edge electron temperature gradients. The low edge density also allows op-

eration with higher core density than would be the case otherwise: the maximum core density in SDC plasmas is  $3 \times$  that predicted by the Sudo empirical scaling for heliotron or stellarator devices [15].

After a sequence of many LID discharges, the wall pumping capability is enhanced, and SDC plasmas with somewhat lower temperatures can then be obtained even without the LID. For longer pulse SDC operation, however, active pumping by the LID is essential. With continuous pellet injection at intervals  $\sim 130$  ms and  $\Delta N = 1 \times 10^{21}$  particles, we have successfully maintained quasi-steady-state SDC operation for nearly 1 s. Perturbations by the pellets on  $W_p$  and the density are  $\sim 15\%$  and can be reduced by optimizing the pellet size for particular discharge conditions.

The temperature gradient in the outer region is determined by anomalous thermal diffusivity. Figure 3 plots the observed edge  $T_e$  gradient versus power input normalized by the edge density ( $P/n_{\text{edge}}$ ). Lowering  $n_{\text{edge}}$  leads to higher edge  $\nabla T$  and hence higher  $T_e(0)$ .

SDC plasma performance depends on the configuration ( $R_{\text{ax}}$ ) partly because of geometry effects. The NBI tangency radius is 3.75 m; thus, the power deposited in the core ( $\rho < 0.4$ ) for  $R_{\text{ax}} = 3.65$  m is a factor of 3 lower than for  $R_{\text{ax}} = 3.75$  m. Also, pellet fuelling is more effective for larger  $R_{\text{ax}}$  and larger core because the pellet particles, injected from the outside, are deposited in the relatively wide range [Fig. 1(a)].

The radial extent of the SDC is determined by the IDB foot location (jump in  $\nabla n$ ), and increases with  $R_{\text{ax}}$  and  $\beta$ . Figure 4(a) plots the measured plasma pressure ( $nT$ ) profiles and the rotational transform profile ( $\iota/2\pi$ ) (calculated with assumption of the pressure profile similar to the observed one) as a function of  $\rho$ , for the SDC configuration with  $R_{\text{ax}} = 3.75$  m. The IDB foot falls at  $\rho = 0.55$ . It is close to the zero-shear radius ( $\rho = 0.63$ ) in the rotational transform for finite- $\beta$  equilibrium. In the low- $\beta$  cases, the shear is nearly zero in the central region and thus definition

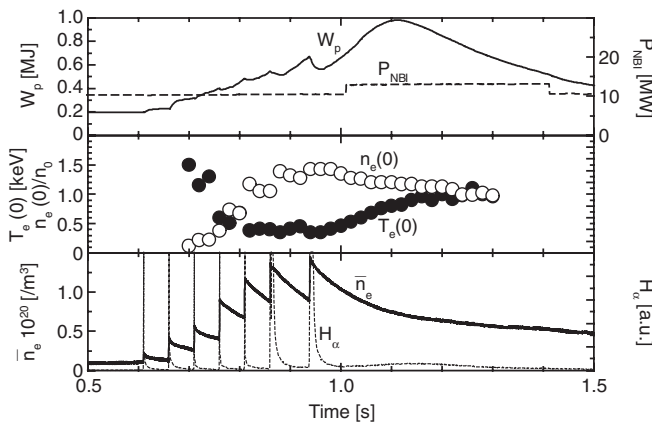


FIG. 2. Time evolution of the plasma parameters in the SDC plasma operation.  $n_0 = 4 \times 10^{20}$  m<sup>-3</sup>.

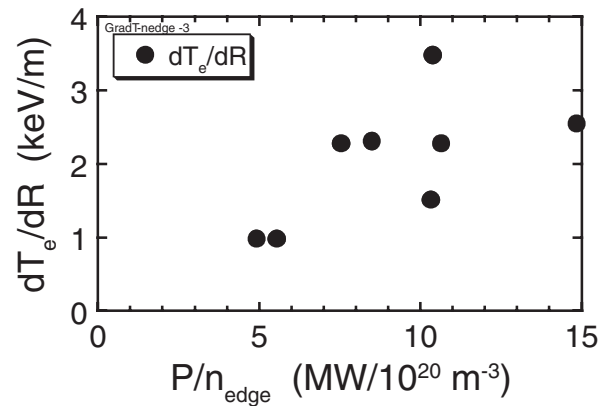


FIG. 3. The temperature gradients in the outer region (at  $R = 4.4$  m) are plotted as a function of  $P/n_{\text{edge}}$  for the SDC operation ( $R_{\text{ax}} = 3.75$  m).  $(1/a)dT/d\rho \sim 0.85dT/dR$ .

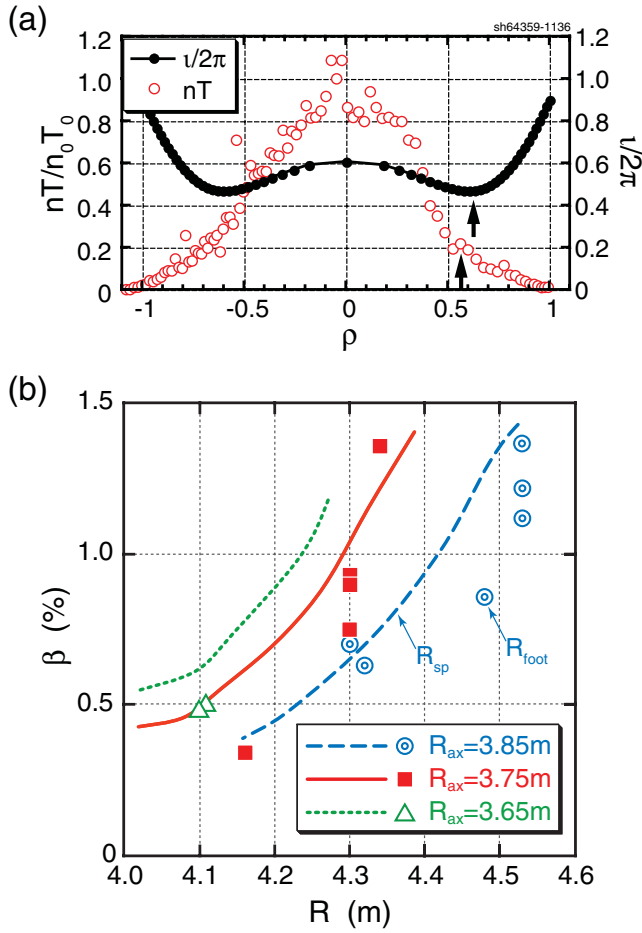


FIG. 4 (color). (a) Typical pressure profile in SDC plasma operation. The location of the IDB foot is  $R_{\text{foot}} = 4.33$  m ( $\rho = 0.55$ ). The location of zero shear  $R_{\text{zs}} = 4.39$  m. (b) With increasing beta and  $R_{\text{ax}}$ , the foot location of the IDB ( $R_{\text{foot}}$ ) increases. The blue, red, and green curves are  $R_{\text{sp}}$  for  $R_{\text{ax}} = 3.85$ , 3.75, and 3.65 m, respectively.

of the zero shear radius ( $R_{\text{zs}}$ ) is ambiguous. To avoid the confusion,  $R_{\text{sp}}$  is defined as the major radius of the intersection point of the lines of tangency to the inner and outer portions of the iota profile. This position separates two distinct regions of the LHD configuration and it is nearly equal to  $R_{\text{zs}}$  [zero shear radius ( $d\iota/dR = 0$ )] for the high- $\beta$  cases. Inside this radius, the rotational transform profile has modest negative or nearly zero shear and a magnetic well, and outside this point, it has positive shear, and a magnetic hill.

This topology is qualitatively insensitive to the shape of  $p(r)$  for fixed magnetic average beta. For fixed vacuum configuration magnetic axis position ( $R_{\text{ax}}$ ), the zero-shear surface moves outward in  $\rho$  with increasing  $\beta$ . For a fixed value of  $\beta$ , the zero-shear radius also moves outward (increasing the volume of the core region) as  $R_{\text{ax}}$  is increased.

Figure 4(b) shows the major radius of the foot locations  $R_{\text{foot}}$  as a function of the average beta for three different

configurations ( $R_{\text{ax}} = 3.65$  m, 3.75 m, 3.85 m). The difference between  $R_{\text{sp}}$  and the experimentally measured  $R_{\text{foot}}$  is less than 0.10 m.

The “standard” configuration ( $R_{\text{ax}} = 3.75$  m) with  $\beta(0) = 4.4\%$ , and the IDB foot at  $\rho = 0.55$  [which corresponds to  $R_{\text{foot}} = 4.33$  m in Fig. 4(b)] yields an SDC with the optimum performance. For the outward shifted configuration ( $R_{\text{ax}} = 3.85$  m) with lower  $\langle\beta\rangle = 0.63$ , a weaker IDB is obtained. As  $\beta$  increases, the SDC grows, and the IDB foot moves outward toward the last closed surface, as shown in Fig. 5.

For the inward shifted case ( $R_{\text{ax}} = 3.65$  m), the SDC is smaller, with the IDB foot at  $\rho = 0.45$  at  $\langle\beta\rangle = 0.5\%$ , corresponding to  $R_{\text{foot}} = 4.10$  m in Fig. 4(b). The “super dense” effect is weaker so far.

The very strong density gradient near the IDB suggests that sheared flows may play a role in confinement improvement, as appears to be the case in tokamaks with strong gradients, such as DIII-D [16].

The ideal MHD stability of these SDC configurations has been examined by using the 3D COBRA stability code [17]. These calculations show that the core region inside the zero-shear radius has direct access to second stability; i.e., the stability margin increases with  $\beta$ . Outside the zero-shear radius, the plasma becomes unstable to ballooning modes at  $\langle\beta\rangle \sim 3\% - 4\%$ . Of course, resistive versions of the modes are expected to appear at lower  $\beta$ . These MHD effects may play a role in improving core confinement, and may also provide a useful mechanism to constrain the plasma pressure in the outer plasma region and thus help maintain the favorable SDC state. We will investigate MHD and turbulence phenomena in future experiments with SDC plasmas.

These results suggest a novel fusion ignition scenario in which an SDC is used to operate at very high density and relatively low temperature. Such a scheme is particularly attractive for helical devices because (a) they do not require current drive (which is most effective at low density),

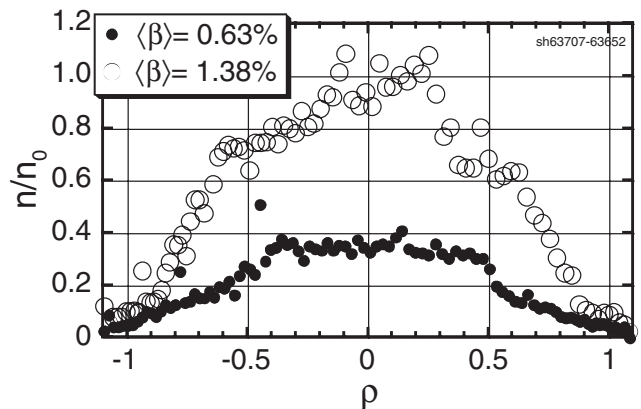


FIG. 5. Density profiles for the outward shifted configuration ( $R_{\text{ax}} = 3.85$  m) with two different values of volume averaged  $\langle\beta\rangle = 0.63\%$  and  $1.38\%$ .

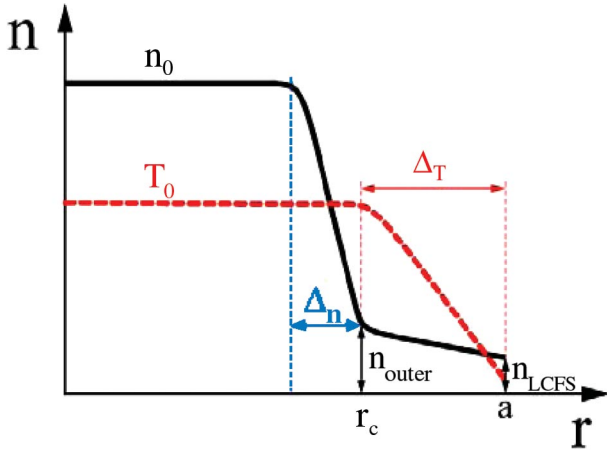


FIG. 6 (color). Schematic profiles for SDC plasma.

and (b) operation at high collisionality reduces the effect of the helical ripple diffusion regime, in which energy and particle losses increase with decreasing collision frequency (increasing temperature).

This scenario (Fig. 6) features a high-density core region (with small diffusivity  $D_0$ ) inside an outer plasma mantle in which the density and pressure are constrained to be quite low, as in our experiments. For ignition, the fusion alpha power must be greater than the conductive plus convective heat fluxes, while power balance holds in the IDB at the core-mantle boundary, i.e.,  $r = r_c$ .

$$\left(5 \frac{D_0}{\Delta_n} + \frac{n_{\text{outer}}}{n_0} \frac{\chi_{\text{outer}}}{\Delta_T}\right) n_0 T_0 S \leq C n_0^2 T_0^2 f(T_0) V.$$

The operating temperature is 6–7 keV, below which the radiative loss exceeds the alpha power. The pellet fueling rate is given by  $S D_0 n_0 / \Delta_n$ , and this particle flow must be also pumped out in steady-state operation. The alpha-particle power density is given by  $C(nT)^2 f(T)$  [ $f(T)$ : a correction factor], and  $V$  and  $S$  are the volume and surface area of the SDC. Low  $D_0$  is important in lowering the convective loss and the particle pumping requirement.

The particle flux induced by pellet injection in the core region is comparable to that in the mantle:

$$D_0 n_0 / \Delta_n \approx D_{\text{outer}} (n_{\text{outer}} - n_{\text{LCFS}}) / \Delta_T$$

and this determines  $(n_{\text{outer}}/n_0)$ . A high value of  $D_{\text{outer}}/D_0$  is crucial to achieving the low  $n_{\text{outer}}/n_0$ , which is the key in reducing the conduction term.

The key challenges for this concept are (1) attaining low values of  $D_0$  and  $(n_{\text{outer}}/n_0) \chi_{\text{outer}}$  (2) ensuring pellet penetration into the core, (3) optimal placement of the IDB.

In summary, a super dense core (SDC) plasma operational regime has been found in LHD discharges. A core region with densities as high as  $4.5 \times 10^{20} \text{ m}^{-3}$  and temperatures of 0.85 keV is confined by an internal diffusion barrier (IDB) with very high-density gradient. The core plasma is fuelled by pellet injection, and the particle edge recycling is reduced by a divertor. These results point to a possible alternative path to very high-density fusion ignition in helical devices.

The authors would like to thank Dr. J. Harris for his valuable discussions on the SDC physics mechanism. They also thank all the colleagues in LHD for their experimental support. This work is supported by NIFS05ULPP506.

- 
- [1] F. W. Perkins *et al.*, Nucl. Fusion **39**, 2137 (1999).
  - [2] F. Wagner *et al.*, Phys. Rev. Lett. **49**, 1408 (1982).
  - [3] T. Fujita *et al.*, Nucl. Fusion **38**, 207 (1998).
  - [4] F. M. Levinton *et al.*, Phys. Rev. Lett. **75**, 4417 (1995).
  - [5] E. J. Strait *et al.*, Phys. Rev. Lett. **75**, 4421 (1995).
  - [6] O. Motojima *et al.*, Phys. Plasmas **6**, 1843 (1999).
  - [7] N. Ohyabu *et al.*, Nucl. Fusion **34**, 387 (1994).
  - [8] N. Ohyabu *et al.*, J. Nucl. Mater. **266–269**, 302 (1999).
  - [9] A. Komori *et al.*, Fusion Sci. Technol. **46**, 167 (2004).
  - [10] T. Morisaki *et al.*, J. Nucl. Mater. **337–339**, 154 (2005).
  - [11] P. Gohil *et al.*, Phys. Rev. Lett. **61**, 1603 (1988).
  - [12] H. Zohm, Plasma Phys. Controlled Fusion **38**, 105 (1996).
  - [13] R. Sakamoto *et al.*, Nucl. Fusion, **41**, 381 (2001).
  - [14] S. Morita *et al.*, *Proceedings of the 14th International Conference on Plasma Physics and Controlled Nuclear Fusion Research, Wurzburg, 1992* (IAEA, Vienna, 1993), Vol. 2, p. 461.
  - [15] S. Sudo *et al.*, Nucl. Fusion **30**, 11 (1990).
  - [16] R. E. Waltz *et al.*, Phys. Plasmas **13**, 052301 (2006).
  - [17] R. Sanchez *et al.*, Comput. Phys. Commun. **141**, 55 (2001).